ACS Catalysis

Research Article

pubs.acs.org/acscatalysis

Computational Identification of Descriptors for Selectivity in Syngas Reactions on a Mo_2C Catalyst

Liwei Li and David S. Sholl*

School of Chemical and Biomolecular Engineering, Georgia Institute of Technology, Atlanta, Georgia 30332-0100, United States

Supporting Information

ABSTRACT: A microkinetic model containing 53 elementary steps based on extensive Density Functional Theory calculations is developed to describe syngas reactions on a Mo_2C catalyst under high temperature and pressure conditions, with the aim of determining the elementary steps that control reaction selectivity. The effects of adsorbate−adsorbate interactions are found to be strong, so these interactions are described using the quasi-chemical approximation. Agreement with experimental observations of selectivity for syngas reactions at P = 30 bar and T = 573 K was found to be good without parametrizing the model in any way to the experimental reaction data. The activation energies of the elementary steps in the model were estimated using a Bronsted−Evans−Polanyi relation, and sensitivity analysis is used to examine the impact of uncertainties in this relation on the selectivity-determining steps of the reaction network. Our results are a useful example of identification of key elementary steps in a complex reaction network for the reactions available with syngas over a heterogeneous catalysis.

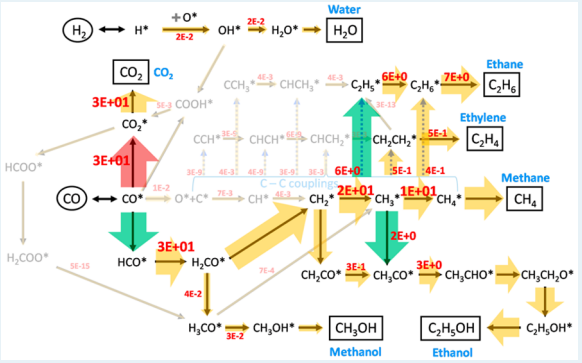

KEYWORDS: *syngas reactions, alcohol synthesis, molybdenum carbides, density functional theory, quasi-chemical approximation, Bronsted−Evans−Polanyi relation*

1. INTRODUCTION

With limited fossil fuel resources, extensive research efforts have been devoted to find alternative building blocks in the chemical industry. Among many candidates, syngas is potentially promising as it can be either derived from conventional sources such as coal and natural gas, or renewable sources like biomass.[1,2] Syngas can be converted to downstream products directly through syngas reactions. However, because these reactions produce a series of products, managing reaction selectivity often turns out to be critical.[3−9]

Molybdenum carbides have been reported in many catalysis applications such as steam reforming,[10−12] Fischer−Tropsch synthesis,[13−17] water−gas shift,[18−20] and higher alcohol synthesis,[21−23] due to their noble-metal-like catalytic properties, relatively low cost, and resistance to poisoning. More interestingly, as a syngas reaction catalyst, molybdenum carbides were found to shift reaction selectivity significantly from hydrocarbons to alcohols when used with alkali promoters.[21,23,24] In principle, understanding the relation between selectivity and catalyst structure could eventually help in designing catalysts selective to a specific product. However, little progress has been made in this endeavor to date due to the complexity of the syngas reaction mechanism.

A number of theoretical studies have been performed for Mo_2C, including examination of structural information,[25−29] adsorption behavior,[25−28] stability,[25,26,29−31] and catalytic performance.[27,32−35] Recently, Medford et al. applied *ab initio* thermodynamics and Density Functional Theory (DFT) to study the stability of surface structures of Mo_2C and adsorption of reactive intermediates as well as C−O bond dissociation on the Mo_2C surface.[36] Pistonesi et al. studied adsorption of alkali metal on Mo_2C surfaces and its effect on CO adsorption and dissociation.[37] Tominaga et al. reported energetics of CO hydrogenation and C−O bond cleavage on molybdenum and cobalt molybdenum carbide catalysts.[38] Most of these studies focus on specific elementary steps, with the inherent assumption that this gives an adequate descriptor of catalyst performance. This could be potentially problematic for several reasons: (1) these steps might not have the lowest activation energy among competing processes; (2) these steps might be the lowest activation-energy steps, but still not necessarily the rate-determining steps (RDS), since kinetically, reaction rates also depend on surface coverage; (3) these steps might be the RDS for certain products, but not necessarily the ones responsible for controlling overall selectivity. Addressing these issues is especially important for a complex reaction system where reaction pathways could be numerous and intricate.

Motivated by these observations, we seek to provide a broad perspective on syngas reaction using a Mo_2C catalyst by describing a complex reaction network and determining which

Received: October 8, 2014
Revised: June 10, 2015
Published: July 24, 2015

DOI: 10.1021/acscatal.5b00419
ACS Catal. 2015, 5, 5174−5185

steps contribute most to the overall reaction selectivity. Specifically, we developed a reaction network containing relevant syngas reactions, including Fischer−Tropsch synthesis, methanol synthesis, ethanol synthesis, and water−gas shift. All the reaction energies in this network were calculated by DFT, whereas activation energies were approximated by Bronsted−Evans−Polanyi (BEP) relations. With these energies as inputs, a microkinetic model was formulated, and the reaction selectivity was computed and compared with experimental results. Finally, sensitivity analysis was applied to determine the overall model's sensitivity on changes of each elementary step. This work gives insights into the reaction mechanism of syngas reactions on Mo_2C catalysts and serves as a useful example of determining descriptors for a complex reaction network.

2. COMPUTATIONAL METHODS

Our plane wave DFT calculations were performed with the Vienna *ab initio* simulation package (VASP).[39−42] We employed the revised Perdew−Burke−Ernzerhof (rPBE) generalized gradient functional[43,44] along with the projector augmented wave (PAW)[45,46] method to describe ionic cores. A plane wave expansion with a cutoff of 400 eV was used for all calculations. Geometries were relaxed using a conjugate gradient algorithm until the forces on all unconstrained atoms were less than 0.03 eV/Å. Spin polarization was not included in our calculations.

For surface structure calculation, a 6 × 6 × 1 Monkhorst−Pack k-point mesh was used for (1 × 1) surface unit cell, which was sufficient to give well-converged energies for the Mo_2C surface. For calculations on a (2 × 2) surface unit cell, the number of k-points was reduced to 3 × 3 × 1. Geometries and energies for gas-phase species were calculated using supercells equivalent to those for the largest slab calculations. When examining adsorption, molecules were placed on only one side of the slab. Dipole corrections were therefore applied in computing all of the energies reported below.[47,48] The adsorption energy, $E_{adsorption}$, of an atom or a molecule was defined by

$$E_{adsorption} = (E_{surface} + E_{adsorbate}) - E_{total} \quad (1)$$

where E_{total} is the total energy of the system containing the adsorbed species, $E_{surface}$ is the total energy for the optimized bare surface, and $E_{adsorbate}$ is the total energy for the adsorbate in the gas phase. With this definition, positive adsorption energies correspond to energetically favored states. For E_{total} and $E_{adsorbate}$, the vibrational modes of adsorbates were computed within the harmonic approximation holding all surface atoms fixed and the zero-point energy of the adsorbate ($\sum_i(h\nu_i/2)$) was added to the DFT calculated energy. Adsorbate coverages were defined by considering a surface with an adsorbed species on every surface molybdenum atom to have coverage of 1 monolayer (ML). This means that placing one adsorbate in a 1 × 1 unit cell gives a coverage of 0.25 ML.

3. RESULTS AND DISCUSSION

3.1. Bulk and Surface Structure of Mo_2C Catalyst. The bulk and surface structures of the molybdenum carbide catalyst modeled in this work are based on the work discussed in a previous study.[26] In that study, the DFT optimized lattice parameters of the hexagonal Mo_2C bulk structure were confirmed to be in good agreement with experimental results. By comparing surface free energy and adsorption energy of alkali metal (K and Rb) atoms for different low-Miller-index surfaces of Mo_2C, the $Mo_2C(001)$ surface was determined to be one of the major surfaces found on Mo_2C particles in equilibrium as well as the one having the greatest affinity and dipole moment for K/Rb atoms. This surface is also known to favor a reconstruction in the absence of adsorbates,[49,50] which results in both Mo-top and C-top sites for adsorption. As we demonstrate below, reaction intermediates adsorb on both Mo-top and C-top sites, so a surface model including Mo-top and C-top sites is more appropriate to represent overall reactivity of Mo_2C than a pure Mo-terminated surface or C-terminated surface. Given all the factors mentioned above, the reconstructed hexagonal $Mo_2C(001)$ surface illustrated in Figure 1 was chosen as a representative Mo_2C surface for further calculations.

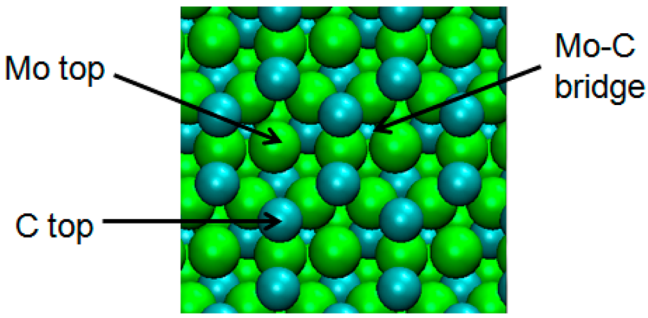

Figure 1. Top view of reconstructed C-terminated Mo_2C (001) surface used in this work. Molybdenum and carbon atoms are depicted in green and cyan, respectively.

3.2. Syngas Reaction Network. As mentioned earlier, syngas reactions on Mo_2C catalysts can generate products including hydrocarbons, alcohols, water, and CO_2. In order to model reaction selectivity, reaction pathways toward all of these products should be considered, which involves water−gas-shift reactions, Fischer−Tropsch (FT) synthesis, methanol synthesis, and higher alcohol synthesis. A tremendous amount of research has been performed to understand the mechanisms of these four types of reactions.[3−7,51−57] In terms of theoretical studies, Cheng et al. performed DFT calculation for FT synthesis on Co,[58,59] Ru, Fe, Rh, and Re surfaces[60] and analyzed the C−C chain growth mechanism.[61,62] Choi et al. performed extensive DFT calculations to investigate ethanol synthesis on Rh(111).[63] Grabow et al. presented a comprehensive mean-field microkinetic model for the methanol synthesis and water−gas-shift reactions.[64] Similar studies have been done by Gokhale et al.,[65] Madon et al.,[66] Grabow et al.,[67] Ferrin et al.,[68] and Mei et al.[69] Although these calculations have been an important tool in elucidating reaction mechanisms, most reaction mechanisms are still under debate, or are only understood for certain catalysts.

In this work, for Fischer−Tropsch synthesis, we include various CH_x-CH_y coupling reactions suggested by a carbene mechanism.[70] For ethanol synthesis, we focus on the most-studied CO-insertion mechanism,[63,71,72] where C_2 oxygenates can be formed by CH_x-CO coupling. For methanol synthesis, although direct CO hydrogenation ($CO + 2H_2 \rightarrow CH_3OH$) is often assumed to be the main reaction mechanism, it was suggested that for Cu-based catalysts, CO_2 hydrogenation ($CO_2^* \rightarrow HCOO^* \rightarrow H_2COO^* \rightarrow H_3COO^* \rightarrow H_3CO^* \rightarrow CH_3OH^*$) was actually responsible for producing metha-

DOI: 10.1021/acscatal.5b00419
ACS Catal. 2015, 5, 5174−5185

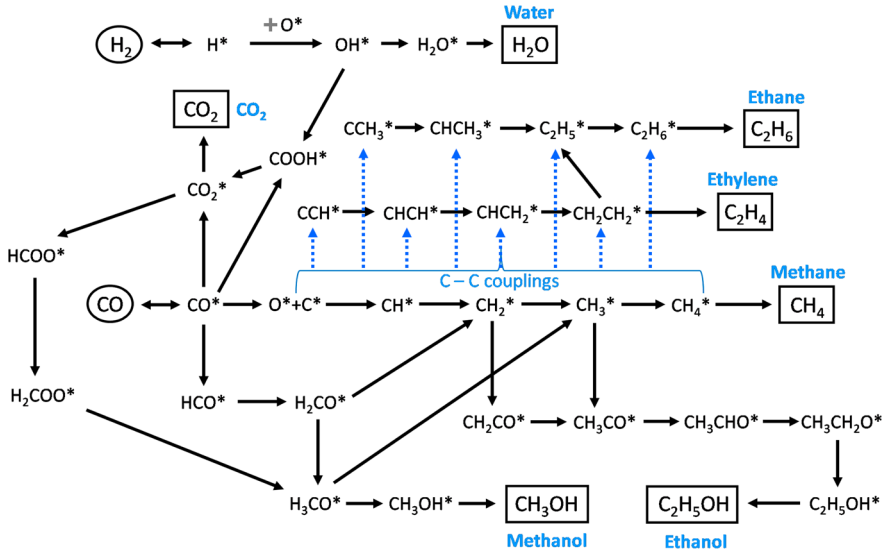

Figure 2. Syngas reaction network examined in this work. Gas-phase species are shown in circles or boxes.

nol.[73−76] Therefore, we include both CO and CO_2 hydrogenation to investigate which one prevails. For water−gas-shift reactions, both redox and carboxyl mechanisms were included in the network. The former assumes CO is oxidized by atomic O produced from H_2O dissociation,[77−79] while the latter involves formation of an intermediate carboxyl group COOH ($CO^* + OH^* \rightarrow COOH^* \rightarrow CO_2^* + H^*$).[65,67] The schematic reaction network is shown in Figure 2. A list of all 53 elementary steps in this network can be found in Table S1 in the Supporting Information.

It should be noted here that we only included products up to C_2 species in this network to save computational cost. From experimental results,[80] it is observed that these species account for more than 80% of the product selectivity on a carbon basis. The only higher products found to be significant were C_3 hydrocarbons (∼10%), which we expect are produced through C_2−C coupling reactions. Therefore, contributions of C_3 hydrocarbons to the hydrocarbon/alcohol selectivity are expected to be lumped in the selectivity of our model network to ethane and ethylene.

3.3. Adsorption of Reaction Intermediates. The adsorption of the 31 reaction intermediates shown in the network in Figure 2 was investigated. In order to have confidence that the most stable adsorption site can be identified, a set of 12 initial adsorbate configurations were examined with a 4 × 3 grid above the (1 × 1) surface unit cell. Most of the intermediates prefer to adsorb on a Mo top, a C top, or a Mo−C bridge site. A list of the most (second most) stable sites for the 31 reaction intermediates can be found in Table S2 in the Supporting Information. The adsorption energies of 9 gas-phase species calculated in a similar way are listed in Table 1.

As expected, CO was found to be the most strongly adsorbed species. As is well-known, DFT calculations of this kind tend to overestimate adsorption energies.[81] To address this point, for CO, we compared our computed adsorption energy with TPD experiment results for Mo_2C in Table 2.[82] Adsorption energies are not directly measured in the TPD experiment, but they can be estimated from TPD peak temperature by the Redhead equation.[83] Two peaks were identified in TPD, which correspond to 1.17 eV/molecule and 0.85 eV/molecule, with

Table 1. Adsorption Energy of Gas Phase Species As Computed with DFT

species	adsorption energy (eV/molecule)
CO	1.46
H_2	1.11
CH_4	0.11
CH_3OH	0.54
H_2O	0.61
CO_2	0.16
C_2H_4	0.55
C_2H_6	0.03
C_2H_5OH	0.05

Table 2. Comparison between Adsorption Energy Calculated from TPD Peak Temperature and DFT-rPBE Functional

adsorption	TPD peak temperature (adsorption energy[a])	computed adsorption energy from DFT
CO on Mo top	450 K (1.17 eV/molecule)	1.46 eV/molecule
CO on C top	328 K (0.85 eV/molecule)	1.18 eV/molecule
difference	(0.32 eV/molecule)	0.28 eV/molecule

[a]Adsorption energy calculated from peak temperature using the Redhead equation with assumed prefactor of 1×10^{13} s^{-1}.

an energy difference of ∼0.3 eV/molecule. In our DFT calculation, CO was found to be adsorbed on Mo top (the most stable site) and C top (the second most stable site), also with ∼0.3 eV/atom energy difference. This supports assigning the two TPD peaks to CO adsorption on Mo top and C top sites. This is also supported by our earlier results that compared vibrational frequencies calculated from DFT with IR experiments.[24]

On the basis of the observations above, we corrected the CO adsorption energy in our model by a factor of 0.8 based on the ratio of the TPD experiment value (1.17 eV/molecule) to the DFT-computed value (1.46 eV/molecule) shown above. To be consistent, we also applied this correction factor to the other eight gas-phase species in the reaction network. TPD experimental results for these eight species are not readily available. For all the other species adsorbed as reaction

DOI: 10.1021/acscatal.5b00419
ACS Catal. 2015, 5, 5174−5185

intermediates, we chose not to apply this correction because the impact of overestimating their adsorption energies will be canceled out in the further reaction enthalpy calculation.

3.4. Approximation of Activation Energy. Because of the large number of transition states that would have to be determined to treat each activated process in our reaction network rigorously, our model applied a Bronsted−Evans−Polanyi (BEP) relation to approximate activation energy for all elementary steps. The BEP relation posits an approximately linear relation between the activation energy and reaction enthalpy:

$$E_a = \alpha \cdot \Delta H + E_0 \tag{2}$$

Several types of bond activation, such as C−C, C−H, C−O bond breaking, on various transition-metal surfaces have been examined extensively to test the validity of the BEP approximation.[84−87] Here, we employed the parameters reported by Michaelides et al.,[84] where for dehydrogenation reactions

$$E_a^{diss} = 0.92\Delta H + 0.87 \tag{3}$$

for diatomic activation reactions

$$E_a^{diss} = 0.97\Delta H + 1.69 \tag{4}$$

and for triatomic activation reactions

$$E_a^{diss} = 0.74\Delta H + 1.03 \tag{5}$$

with all energies in eV. From the principle of reversibility, the activation energy for bond association can be calculated by

$$E_a^{diss} = E_a^{asso} + \Delta H \tag{6}$$

For each elementary step (A* + B* → C* + D*), the reaction enthalpy, ΔH was calculated by

$$\Delta H = E_{C*} + E_{D*} - E_{A*} - E_{B*} \tag{7}$$

where $E_{adsorbate*}$ can be obtained from DFT calculations.

It should be noted that the correlation used here was developed for transition-metal surfaces, rather than transition-metal carbides. Thus, when elementary steps happen on a surface carbidic site, proper parameters should be chosen carefully. For example, diatomic activation on the carbidic site used the triatomic activation parameters shown above. Although in principle, parameters for transition-metal carbide surface should be developed, this is a useful way to rapidly estimate activation energies for transition-metal carbide surfaces. A list of activation energy calculated using the approach above for all steps can be found in Table S1 in the Supporting Information.

3.5. Microkinetic Model. *3.5.1. Quasi-Chemical Approximation.* With all the energetics available, we can compute reaction rates with a microkinetic model. The most widely applied models for this goal are mean field (MF) and kinetic Monte Carlo (kMC) models.[88] Kinetic Monte Carlo requires predefining the rate of each process (adsorption, reaction, diffusion, etc.) at certain local ordering conditions (interaction with nearby species). We chose not to use kMC because of the complexity of the reaction network we are considering. It was important, however, to adopt an approach beyond the MF level to account for adsorbate−adsorbate interaction. To this end, we used the quasi-chemical approximation (QCA),[89−91] which assumes there is chemical equilibrium within redistribution of adsorbed species as shown in Figure 3.

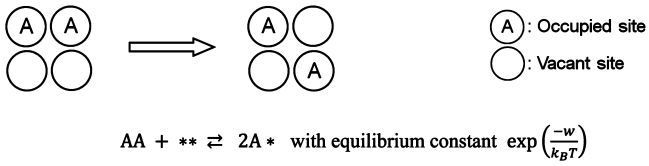

Figure 3. Schematic showing the quasi-chemical approximation.

To use the QCA, the interaction energy w between nearest neighbors must be defined. Our model includes 31 distinct adsorbates. For simplicity, w is approximated as the interaction energy between dominant species on the surface. As shown later in the results section, oxygen was found to be the dominant species on the surface under typical experimental conditions. Therefore, the interaction energy between adsorbed oxygen atoms on the Mo_2C surface was calculated as 0.244 eV by comparing the energy difference between the case of two oxygen atoms adsorbed on neighbor sites and the case of two isolated oxygen atoms on the Mo_2C surface. For simplicity, this energy was used as the value of w for all adsorbed species. The effect of interaction on adsorption, desorption and surface reactions is discussed below.

3.5.2. Adsorption, Desorption, and Surface Reaction Rates. For adsorption of a gas-phase species, the rate is defined in kinetic theory by[92]

$$r_{ads} = \sigma(1 - \sum \theta_i) e^{-E_{a,ads}/k_B T} \cdot \frac{P}{\sqrt{2\pi m k_B T}} \tag{8}$$

where σ is the steric factor which represents the probability that a molecule possessing sufficient energy $E_{a,ads}$ and colliding with a vacant site will adsorb, $E_{a,ads}$ is the activation energy of adsorption process, P is the partial pressure of the adsorbing species, m is the mass of the species, k_B is Boltzmann's constant, and T is the temperature. The term $(1 - \sum\theta_i)$, where θ_i is the fractional surface coverage of species i, represents the probability that a collision occurs with an empty site. In this work, σ is assumed to be 1, and $E_{a,ads}$ is zero by assuming the adsorption is nonactivated process.

For desorption, the rate is defined by[92]

$$r_{des} = \nu L \theta_i e^{-E_{a,des}/k_B T} \tag{9}$$

where ν is the vibrational frequency, assumed to be 1×10^{13} s^{-1}, L is the site density, and $E_{a,des}$ is the activation energy for the desorption process, which is taken to be equal to the adsorption energy E_{ad}.

Interaction between adsorbed species can be important in a desorption process. For instance, with strong repulsive interaction, it is expected that desorption will happen more easily at higher surface coverage. Thus, based on QCA, a correction factor g was applied to desorption rate expression.

$$r_{des} = \nu L \theta_i e^{-E_{a,des}/k_B T} \cdot g \tag{10}$$

Here, g is a function of nearest neighbor interaction energy w, the vacant site coverage θ_*, and number of nearest neighbor sites z as[91]

$$g = \left[\frac{2 - 2(1 - \theta_*)}{1 + \beta - 2(1 - \theta_*)} \right]^z \tag{11}$$

where

DOI: 10.1021/acscatal.5b00419
ACS Catal. 2015, 5, 5174−5185

$$\beta = \left[1 - 4\theta_*(1-\theta_*)\left(1 - \exp\left(\frac{-w}{k_B T}\right)\right)\right]^{1/2} \quad (12)$$

This correction keeps the desorption rates as a closed form equation, which makes the rates easy to use in the calculations below. To demonstrate the importance of the correction factor, we plotted g as a function of surface coverage θ in Figure 4

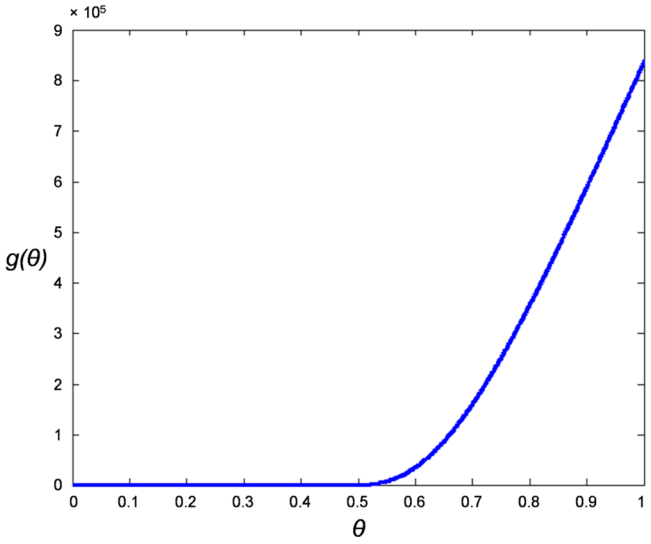

Figure 4. QCA correction factor g as a function of surface coverage θ (Interaction energy w = 0.244 eV and T = 573 K).

using the interaction energy defined above (w = 0.244 eV) at T = 573 K. When the surface coverage is low (<0.5), the adsorbates can be well distributed on the surface without interacting with each other. Therefore, the correction factor g is approximately equal to 1 and effectively no correction is made to the desorption rate term. In contrast, when the surface coverage is high (>0.5), the adsorbates on the nearest neighbored sites start to repel each other, which consequently allows them to desorb more easily. As seen in the right part of the Figure 4, the correction factor g grows rapidly with surface coverage θ and can eventually enhance the desorption rate by a factor as large as $\sim 10^6$.

We compared the performance of MF, QCA, and Monte Carlo models for a simple adsorption/desorption process, finding that the QCA description is accurate in many regime where the MF calculations were inaccurate. Also, our results showed that QCA is one of the key factors making our model accurately predict reaction selectivity. To better demonstrate this point, we provided a numerical example of comparing computed reaction selectivity for models with and without QCA in Table S3. Details of these calculations can be found in the Supporting Information.

For surface reactions, the rate was defined by Transition State Theory as[92]

$$r_i = A\exp\left(\frac{-E_{act,i}}{k_B T}\right) \quad (13)$$

Here, r_i is the rate constant of step i, A is a pre-exponential factor approximated as 10^{13} s^{-1} for all the elementary steps, which assumes the overall reaction rate is dictated by activation energy rather than the pre-exponential factor. $E_{act,i}$ is the activation energy of step i. Although adsorbate−adsorbate interaction can influence surface reaction rates, we treated these reactions at a MF level for simplicity.

3.5.3. Governing Equations and Solution Technique. With adsorption, desorption and surface reaction rates defined, the derivative of surface coverage over time for each species was defined as

$$\frac{d\theta_i}{dt} = (\text{rate of formation of species } i) - (\text{rate of consumption of species } i) \quad (14)$$

Traditional methods of solving rate equations, such as Langmuir−Hinshelwood (L−H) model or the Hougen−Watson (H−W) model,[92] involve simplifying reaction sequence to derive an analytical close-form rate expression. This often requires assuming a specific step to be the rate-determining step (RDS). For example, the L−H model assumes a RDS surface reaction governs the rate and all adsorption/desorption steps are quasi-equilibrated. These models are often good enough to correlate experimental data for simple reactions with a single linear sequence.

For complex reactions, where there are reactions split into multiple linear sequences and interconnections between different sequences, a closed-form rate expression cannot readily be derived. Moreover, as the goal of this work is to determine rate and selectivity limiting steps, it is preferable to make no assumptions regarding these steps. Thus, we solved the above equations numerically without imposing assumptions on the reaction mechanism. At steady state, the derivative of surface coverage over time is zero for each surface species, which gives N (but $N-1$ independent) equations, plus with surface site balance $\sum_1^N \theta_i = 1$. Here, N is the number of surface species including vacant site. This defines an algebraic equation set with N equations and N unknown surface coverages that was solved numerically with Matlab's fsolve function. Because the rate constant terms in the equation set could differ by orders of magnitude, variables were scaled to equalize their effect on the objective and constraint functions. As a nonlinear optimization problem, an initial estimate of the surface coverages is needed. This estimate was obtained from time evolution of θ_i by solving $(d\theta_i/dt)$ with the Matlab solver for stiff ODEs, assuming that at t = 0, the surface was complete empty (θ_* = 1). A mass balance was performed to confirm equations were solved self-consistently.

3.6. Results. *3.6.1. Surface Coverage.* The steady-state surface coverage solved from the microkinetic model under typical experimental conditions is shown below in Table 3. A list of coverages for all 32 species can be found in Table S4 in the Supporting Information.

Under the chosen conditions (573 K, 30 bar of syngas, CO/H_2 = 1:1), oxygen was found to be the most abundant species on the surface at steady state. This is an interesting but not entirely surprising result. There have been multiple studies reporting that a molybdenum oxycarbide phase could be formed *in situ* over Mo_2C catalysts under syngas reaction conditions.[93−98] Our results shows that surface oxygen originating from CO tends to accumulate on Mo_2C catalytic surface when a steady state is reached. It is important to note that the total surface coverage is high; less than 3% of the surface sites are unoccupied.

3.6.2. Selectivity. With the surface coverage at steady state, the production rates of six gas-phase products were calculated. The product selectivities, defined as the percentage of specific

DOI: 10.1021/acscatal.5b00419
ACS Catal. 2015, 5, 5174−5185

Table 3. Steady-State Surface Coverages at Typical Experimental Condition (573 K, 30 bar of Syngas with CO/H_2 in an 1:1 ratio)

no.	species	coverage
1	O*	62.3%
2	CO*	21.5%
3	CH_2*	3.2%
4	*	2.9%
5	CHO*	2.1%
6	CH_3CH_2O*	1.9%
7	CH_3*	1.8%
8	C_2H_5*	1.8%
9	CH_3CO*	1.8%
10−32	other 23 species	0.7%
	sum	100%

production rate within the overall production rate, are listed in Table 4. In order to compare with experimental results, we reported the computed selectivity implementing a carbon %-based notation used in the experimental data of Shou et al.[80] The selectivity to product i is based on the total number of carbon atoms in the product and is therefore defined as

$$\text{selectivity}\ (\%) = \frac{n_i M_i}{\sum n_i M_i} \times 100 \qquad (15)$$

where n_i is the number of carbon atoms in product i and M_i is the percentage of product i.

As can be seen in Table 4, our computed selectivities are in good agreement with experimental results. As expected, besides CO_2 as a major byproduct, the unpromoted Mo_2C catalyst primarily produces hydrocarbons (80% ∼ 90% selectivity on CO_2 free basis) rather than alcohols. Most of the hydrocarbons were in form of paraffins, although some olefins were also observed. It is important to emphasize that our model was not fitted in any way to the experimental data shown in Table 4. The consistency between the predictions of our first-principle-based model and this experimental data gives us confidence that our model can be used in a predictive sense for this complex catalytic system. We understand that a systematic test of the model against experimental results at different conditions would be preferred to validate our model. However, with limited experimental data, we are only able to test our model at the benchmark condition of 573 K, 30 bar, and a limited range of temperatures and pressures, which will be covered in the next section.

The importance of accounting for adsorbate−adsorbate interactions is highlighted in Table S3, which compares the selectivities predicted using our reaction network with the QCA (the approach taken above) with results from the same network at the mean field level. Because of the high coverage of the surface under these conditions, there is a substantial difference between the MF and QCA-based results.

3.6.3. Effect of Temperature and Pressure on Selectivity. With good agreement reached at benchmark reaction condition (573 K, 30 bar of syngas with CO/H_2 = 1:1) used experimentally, the performance of our model was further tested under different temperature and pressure conditions, as shown in Table 5 and Table 6.

Table 5. Selectivities of Total Hydrocarbons and Total Alcohols at Different Temperatures (on CO_2-Free Basis) Using 30 bar of Syngas with CO_2/H_2 = 1:1

species	548 K	573 K	598 K
total hydrocarbons	82.6%	82.9%	83.3%
total alcohols	17.4%	17.1%	16.7%

Table 6. Selectivities of Total Hydrocarbons and Total Alcohols at Different Pressures (on CO_2-Free Basis) at T = 573 K Using Syngas with CO_2/H_2 = 1:1

species	20 bar	30 bar	40 bar
total hydrocarbons	84.5%	82.9%	81.8%
total alcohols	15.5%	17.1%	18.2%

Our model shows that with increasing temperature, the selectivity of total hydrocarbons increases at the expense of selectivity to alcohols. This is consistent with the trend observed experimentally,[99] where it was proposed that alcohol synthesis reactions are more exothermic than Fischer−Tropsch synthesis. The trend of hydrocarbon and alcohol selectivities as a function of pressure also match the experimental results,[99] where higher syngas pressure made the catalysts more selective to alcohols. This could be explained as a surface coverage effect, where at higher pressure, more CO* enhances alcohol production through a CO-insertion mechanism.

3.6.4. Reaction Rates at Steady State. The comparison above with experimental results indicates that our reaction network usefully describes the mechanism of syngas reactions over Mo_2C. To clearly demonstrate the reaction mechanism, we calculated the rates of all individual elementary steps in the network at steady state under the benchmark reaction condition (573 K, 30 bar with CO/H_2 = 1:1), and plotted them in Figure 5. The numbers in red in Figure 5 are the elementary step rates in units of molecule per second per site. For simplicity, steps along the same reaction route with the same rate are only labeled once. To better visualize our results,

Table 4. Comparison between Computed and Experimental Selectivities, Using Experimental Data from Shou et al.[80]

species	computed selectivity	experimental selectivity[80]
CO_2 selectivity (on a CO_2-free basis)	47.7%	46%
total hydrocarbons	82.9%	89%
CH_4	36.7%	33%
C_2+ hydrocarbons	46.2% (3.1%C_2H_4 + 43%C_2H_6)	56%
total alcohols	17.1%	11%
CH_3OH	0.2%	4.9%
C_2+ alcohols	16.9%	6.1%

Reaction condition at 573 K, 30 bar of syngas with CO/H_2 = 1:1

DOI: 10.1021/acscatal.5b00419
ACS Catal. 2015, 5, 5174−5185

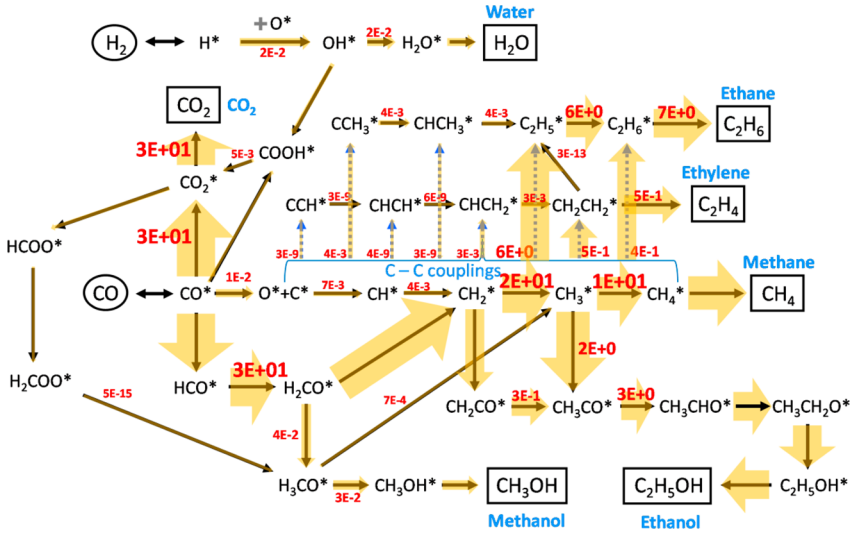

Figure 5. Rates of elementary steps in the reaction network at steady state. Gas-phase reactants (products) are shown in circles (rectangles). Elementary step rates (in red) are in unit of molecule per second per site.

Table 7. Degrees of Rate Control for Selected Steps under Reaction Condition at 573 K, 30 bar of Syngas with CO/H_2 = 1:1

	CH_4	CO_2	C_2H_6	C_2H_5OH
$CH_2^* + H^* \rightarrow CH_3^* + *$	**0.46**	0.03	-0.10	0.14
$CH_3^* + H^* \rightarrow CH_4^* + *$	**0.59**	0.05	-0.34	-0.34
$CO^* + H^* \rightarrow HCO^* + *$	0.24	0.02	0.38	**0.97**
$CO^* + O^* \rightarrow CO_2^* + *$	0.08	**0.94**	-0.25	**-0.64**
$CH_3^* + CO^* \rightarrow CH_3CO^* + *$	-0.15	-0.06	-0.14	**0.74**
$CH_2^* + CH_3^* \rightarrow CH_2CH_3^* + *$	-0.35	0.03	**0.44**	-0.32

Weak inhibiting step (-0.7<value<-0.4)
Weak promoting step (0.4<value<0.7)
Strong promoting step (value > 0.7)

All the other 47 elementary steps have degree of rate control smaller in magnitude than 0.05.

we drew arrows to qualitatively represent these rates, where a broader arrow indicates a larger rate. As shown in Figure 5, certain pathways within the overall network dominate. For instance, for water−gas-shift reactions, the pathway going through CO* (redox mechanism) is 10^4 times faster than the one via COOH* (carboxyl mechanism). Similarly, for methanol production, although CO_2 hydrogenation mechanism has been reported to be dominant on a Cu-based catalyst,[64,73,75,76] our results suggest that methanol is mainly produced through a CO hydrogenation mechanism on Mo_2C.

One issue receiving growing attention recently is how adsorbed CO dissociates on catalyst surfaces. It has long been considered that CO* directly dissociates into C* and O*.[70,71,100] However, evidence in recent years, both theoretically and experimentally,[101−103] indicates that CO* can dissociate with the assistance of hydrogen. H-assisted CO dissociation involves a two-step process: adsorbed CO is first hydrogenated to H_xCO^*, and then dissociates to CH_x^* and O*. Our results are an example of this phenomenon, where H-assisted CO dissociation is dominant over direct CO dissociation.

CH_2^* is found to be a major intermediate produced from H-assisted CO dissociation. CH_2^* can be coupled with other CH_x^* intermediates to produce C_2 hydrocarbons. Our results show that C_2 hydrocarbons are mainly produced from coupling of $CH_2^*+CH_3^*$ rather than couplings of CH_x species with lower hydrogen content such as CH*+CH*. Finally, for ethanol synthesis, our results showed that CO insertion mechanism through CH_3^* is the primary reaction pathway while CO insertion through CH_2^* also plays an important role.

3.6.5. Sensitivity Analysis—Production Rate. The previous section has qualitatively discussed the dominant reaction pathways in our network. This eliminates a large number of steps from consideration as the events that control the catalyst performance. To further determine which elementary steps in these pathways are the most kinetically rate-limiting, we performed a sensitivity analysis on our reaction network. This approach was introduced by Campbell as "degree of rate control" analysis.[104,105] The basic idea is to increase/decrease the rate constant of a step by a small amount and calculate the resulting fractional change in the overall rate. The step whose increase/decrease leads to the greatest increase/decrease in the overall rate is then considered the most rate-controlling. Campbell defined the degree of rate control by

$$X_{\mathrm{rc},i} = \left(\frac{k_i}{r}\right)\left(\frac{\delta r}{\delta k_i}\right) \tag{16}$$

where, $X_{\mathrm{rc},i}$ is the degree of rate control of step i, k_i is the rate constant of step i; r is the reaction rate of targeted product; δr and δk_i are the differential changes of corresponding reaction rate and rate constant.

As our model was solved by numerical methods, the disturbance introduced in sensitivity analysis δk_i should be small enough to make a small impact on the model results but large enough to be differentiated from numerical uncertainty in

DOI: 10.1021/acscatal.5b00419
ACS Catal. 2015, 5, 5174−5185

Table 8. Degrees of Selectivity Control for Selected Steps

	CH_4	CO_2	C_2H_6	C_2H_5OH
$CH_3^* + H^* \rightarrow CH_4^* + *$	**0.56**	0.02	-0.38	-0.37
$CO^* + H^* \rightarrow HCO^* + *$	-0.11	-0.33	0.03	**0.62**
$CO^* + O^* \rightarrow CO_2^* + *$	-0.20	**0.65**	**-0.53**	**-0.92**
$CH_3^* + CO^* \rightarrow CH_3CO^* + *$	-0.13	-0.04	-0.12	**0.76**
$CH_2^* + CH_3^* \rightarrow CH_2CH_3^* + *$	-0.36	0.02	**0.43**	-0.33

Strong inhibiting step (value <-0.7)
Weak inhibiting step (-0.7<value<-0.4)
Weak promoting step (0.4<value<0.7)
Strong promoting step (value > 0.7)

All the other 48 elementary steps have degree of selectivity control smaller in magnitude than 0.05.

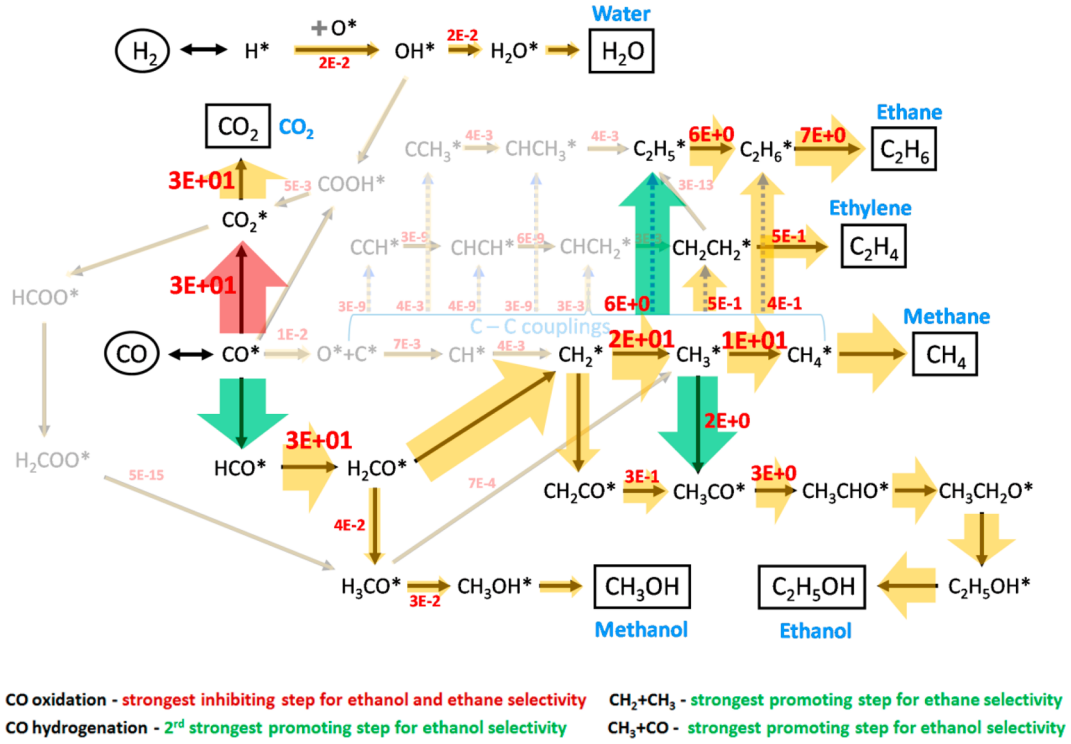

Figure 6. Important selectivity-determining steps within the main reaction mechanism illustrated in Figure 5.

our calculations. We used $(\delta k_i/k_i)$ = 1%, 3%, 5%, 8%, and 10% and tested their performance for a small group of elementary steps. We found that 1% was too small, although 10% was too large. All results below were calculated using $(\delta k_i/k_i)$ = 5% for the degree of rate control, as summarized in Table 7.

By definition of the degree of rate control, steps with a positive degree of rate control indicate the targeted production rate is promoted by these steps, whereas a negative degree of rate control means the targeted production rate is inhibited by these steps. The larger the absolute value of the degree of rate control, the more rate-controlling the step is. Thus, by performing degree of rate control analysis, we quantitatively identified which steps are rate-controlling. In Table 7, we listed elementary steps having degrees of rate control larger than 0.4 for the production of CH_4, CO_2, C_2H_6, and C_2H_5OH. Of the 53 elementary steps in the network, only 6 of them are rate limiting. Specifically, for ethanol production, hydrogenation of CO* is found to be the strongest promoting step. Oxidation of CO* is the strongest inhibiting step for ethanol production but the strongest promoting step for making CO_2. These findings suggest that reactions involving CO* as the starting point of the reaction network greatly influence the overall activity of syngas reactions. Whether adsorbed CO is hydrogenated or oxidized directly correlates with production of alcohols and CO_2 respectively. Similarly to CO*, CH_3* is another important splitting point for producing ethane and ethanol. As a promoting step for making ethane, $CH_2^* + CH_3^*$ is found to be the dominant step for C−C coupling among eight distinct CH_x-CH_y coupling steps in the network. On the other hand, $CH_3^* + CO^*$ is a strong promoting step for making ethanol. Finally, $CH_3^* + H^*$ and $CH_2^* + H^*$ are the strongest two promoting steps for methane production.

3.6.6. Sensitivity Analysis—Selectivity. Above, we determined six elementary steps controlling production rates in syngas reactions. However, as discussed earlier, we are primarily interested in characterizing the steps that control the reaction selectivity. Therefore, we further applied sensitivity analysis to the reaction selectivity. Similar to the idea of degree of rate control used in previous section, we define the degree of selectivity control as

$$Y_{sc,i} = \left(\frac{k_i}{s}\right)\left(\frac{\delta s}{\delta k_i}\right) \quad (17)$$

where $Y_{sc,i}$ is the degree of selectivity control of step i, k_i is the rate constant of step i; s is the reaction selectivity of the

DOI: 10.1021/acscatal.5b00419
ACS Catal. 2015, 5, 5174−5185

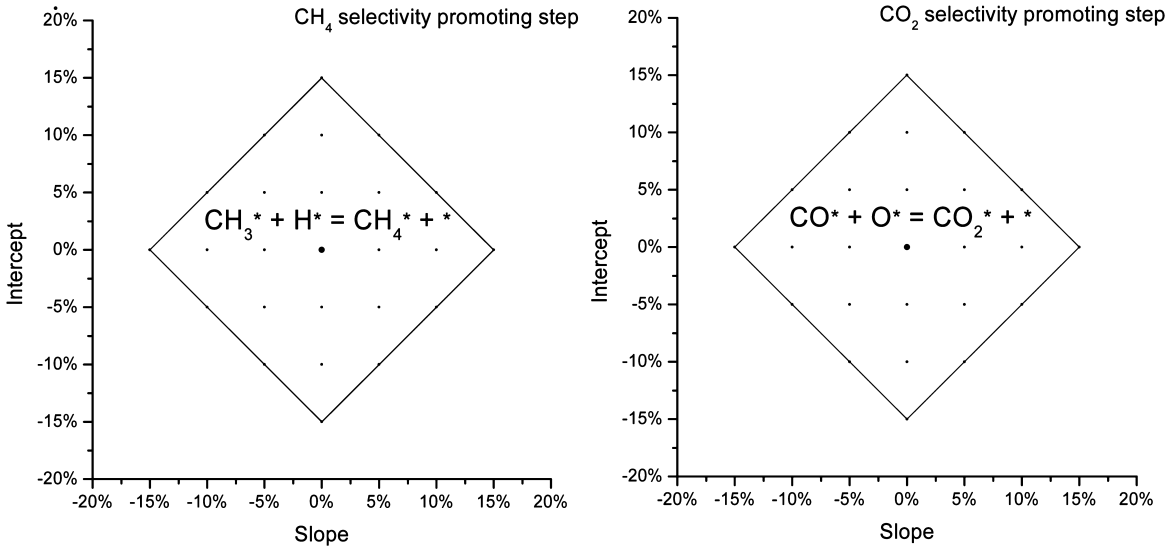

Figure 7. Selectivity-promoting step for CH_4 and CO_2 at different levels of error on the slope and intercept terms in the BEP relation. The solid lines indicate the range of errors analyzed.

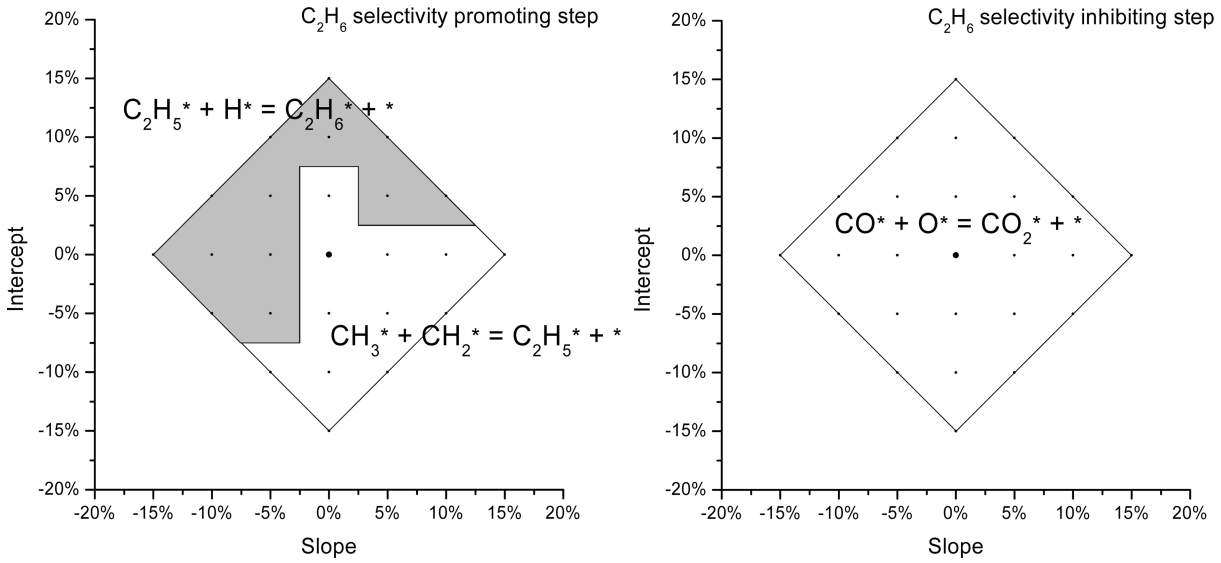

Figure 8. Selectivity-promoting and inhibiting steps for ethane at different levels of error on the slope and intercept terms in the BEP relation. The solid lines indicate the range of errors analyzed.

targeted product; δs and δk_i are differential changes of corresponding reaction selectivity and rate constant.

The results of degree of selectivity control are shown in Table 8. Comparing to the results in Table 7, most of the rate-determining steps are also the selectivity-determining steps. However, the meanings behind selectivity-determining and rate-determining are not entirely the same. One elementary step may promote the production of a product while inhibiting its selectivity because it promotes the production of other competing products even more. For example, as shown in Table 7, CO hydrogenation turned out to increase the rates of all four products, but as shown in Table 8, it inhibits selectivities of methane and CO_2. The hydrogenation of CH_3* is the strongest promoting step for CH_4 selectivity while it has negative impacts on the selectivities for C_2H_6 and C_2H_5OH. This is reasonable because they share CH_3* as an important reaction intermediate, where more CH_3* going toward CH_4* will result in less of them being produced as C_2 species. Similarly, CO hydrogenation (CO* + H*) and CO oxidation (CO* + O*) are also competing steps in the reaction network. The former step promotes C_2H_5OH selectivity and inhibits CO_2 selectivity while the latter enhances CO_2 production and impedes all the other products. These selectivity-determining steps are illustrated in Figure 6. As can be seen in the figure, within the main reaction mechanism shown in Figure 5, in general the elementary steps at the intersections of the reaction network are important in determining the reaction selectivity.

Another interesting finding is the selectivity controlling step of ethanol. CO insertion (CH_3*+ CO*) turned out to be the strongest promoting step for ethanol selectivity, as well as the only step that promotes ethanol production and inhibits ethane production. This suggested a possible explanation for selectivity shift from hydrocarbons to alcohols on alkali promoted Mo_2C catalysts observed experimentally. Our results imply that CO

DOI: 10.1021/acscatal.5b00419
ACS Catal. 2015, 5, 5174−5185

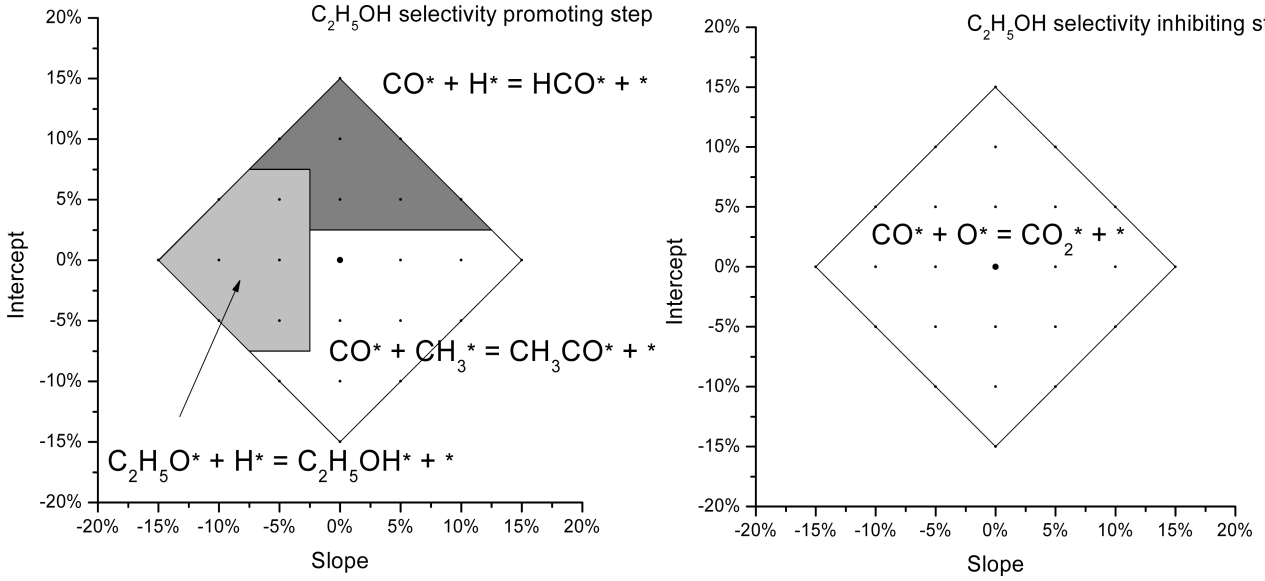

Figure 9. Selectivity-promoting and inhibiting steps for ethanol at different levels of error on the slope and intercept terms in the BEP relation. The solid lines indicate the range of errors analyzed.

insertion could be promoted by alkali promoters and thus the overall selectivity is shifted from hydrocarbons to alcohols.

3.6.7. Model Robustness Analysis over BEP Relation. As mentioned earlier, our model applied a BEP relation to approximate the activation energy for all surface elementary steps. It is useful to ask how accurate the BEP relation is and whether this affects the validity of our conclusion. As the BEP relation is by definition an approximation without considering how reactions take place at a detailed level, a certain margin of error in this approximation is expected. Because the motivation of this work is to identify rate/selectivity controlling steps in a complex network, we aimed to understand the impact of the BEP relation on these steps.

To examine the robustness of this model against error, we deliberately manipulated both the slope and intercept terms of the BEP relation, and we repeated all the calculations above to calculate the degree of selectivity control. Specifically, we introduced errors to the slope and intercept terms in eqs 3, 4, and 5, at levels of ±5%, ± 10%, and ±15%, as follows:

$$E_a = \alpha\cdot(1 + x)\cdot\Delta H + E_0\cdot(1 + y)$$
$$x, y = \pm 5\%, \pm 10\%, \pm 15\%$$
$$|x| + |y| \ll 15\% \quad (18)$$

In Figure 7, the selectivity-promoting step for CH_4 was shown for the range of conditions we analyzed. CH_3*+H* was found to be the only selectivity-promoting step over the whole range of conditions. This is an encouraging result, suggesting that a quantitative uncertainty in a BEP relation may not influence qualitatively identifying the selectivity-determining step of a reaction. Similarly, for CO_2 selectivity, CO* + O* remains to be the strongest promoting step, as determined in Table 8. On the other hand, the selectivity-determining steps for ethane and ethanol are more complicated. In Figure 8, the strongest promoting and inhibiting steps for the ethane selectivity are illustrated. Although CO* + O* is still the strongest inhibiting step for all conditions we examined, with an overestimated intercept term and an underestimated slope term in the BEP relation, C_2H_5*+H* became the strongest promoting step for ethane selectivity. In other situations, CH_3* + CH_2* is the strongest promoting step. In Figure 9, similar results were obtained for ethanol case, where three elementary steps: CO hydrogenation (CO* + H*), CO insertion (CO* + CH_3*) and C_2H_5O hydrogenation (C_2H_5O* + H*) could be the strongest selectivity-promoting step based on the error associated with the BEP relation. These results suggest that our conclusions in previous sections could be influenced by the errors in the BEP relation to some extent. Nevertheless, this analysis still narrows the list of possible selectivity-determining steps to a few elementary steps.

4. CONCLUSIONS

This work provides a useful example of screening selectivity-determining elementary steps in a complex reaction network on a heterogeneous catalyst. Our model mainly employs energy inputs from DFT calculations. DFT-computed adsorption energies for gaseous products were corrected to be consistent with experimental TPD results. Activation energies for surface reactions were approximated from a BEP relation. To consider interactions between surface intermediates, we applied the quasi-chemical approximation to calculate contribution from nearest neighbored adsorbates while keeping the whole approximation in closed form. Further, kinetic theory and transition-state theory were used to derive the rate equations, and the whole equation set was numerically solved without imposing any assumptions on the reaction mechanism. To validate our methodology, our computed selectivities were compared with experimental selectivities at various temperatures and pressures, where excellent agreement was reached. Finally, sensitivity analysis was performed to determine individual elementary step's contribution to the overall selectivity. We are able to conclude with very few steps that are selectivity-determining. As a long-term goal, these steps can be used as descriptors and could potentially help the rational design of catalysts selective to specific products.

In terms of mechanistic insights into syngas reactions on Mo_2C catalysts, our results suggested that H-assisted CO dissociation was dominant over the direct CO dissociation on

DOI: 10.1021/acscatal.5b00419
ACS Catal. 2015, 5, 5174−5185

Mo_2C under the experimental conditions we used. Within a reaction network including 53 elementary steps, 5 steps control the selectivities of CH_4, CO_2, C_2H_6 and C_2H_5OH. CO oxidation (CO* + O*) was found to be the strongest inhibiting step for C_2H_6 and C_2H_5OH selectivity. CO insertion (CO* + CH_3*) and CO hydrogenation (CO* + H*) are the strongest two promoting steps for C_2H_5OH selectivity, while CH_2* + CH_3* was suggested to be the strongest selectivity-promoting step for C_2H_6 production. As the only step promoting ethanol selectivity while inhibiting ethane selectivity, CO insertion could be potentially responsible for the selectivity shift from hydrocarbons to alcohols upon addition of alkali promoters observed in experiments.

Although the conclusions above are specifically drawn for a Mo_2C catalyst, some of them can be generalized and potentially helpful to understand syngas reactions on other types of catalysts. First, investigating product selectivity of syngas reactions is a complex problem, and it requires developing a reaction network to consider all the relevant reactions. For example, FT synthesis, methanol synthesis, alcohol synthesis, and water−gas-shift chemistry should all be included. Second, elementary steps controlling the production rate and selectivity are generally the slowest steps in the fastest reaction pathways. This raises the complication that sometimes an elementary step may be fast enough to create a dominant reaction pathway while too fast to be the controlling step for the pathway. For instance, H-assisted CO hydrogenation turned out to be critical because it provided a faster pathway to break C−O bond than direct CO dissociation. However, our results suggested it is not a rate-controlling step because it is not the slowest step in the overall H-assisted CO dissociation pathway. Finally, steps where the reaction network splits into different products are important to product selectivity and thus should be closely examined. As shown in this work, reactions involving CO* play an important role as whether CO* is oxidized, hydrogenated directly influences selectivity of CO_2 and hydrocarbons. Similarly, CH_3* is another vital reaction intermediate because it reacts with CO*, H*, or CH_2* and therefore could potentially determine overall selectivities toward ethanol, methane and ethane.

■ ASSOCIATED CONTENT

Supporting Information

The Supporting Information is available free of charge on the ACS Publications website at DOI: 10.1021/acscatal.5b00419.

Elementary steps considered in syngas reaction network and adsorption energies and geometries of surface species (PDF)

■ AUTHOR INFORMATION

Corresponding Author

*E-mail: david.sholl@chbe.gatech.edu.

Notes

The authors declare no competing financial interest.

■ ACKNOWLEDGMENTS

Financial support from The Dow Chemical Company is gratefully appreciated. Helpful discussions with Dr. Chris Jones, Dr. Robert Davis, Dr. Heng Shou, Dr. David Barton, and Dr. Daniela Ferrari are also gratefully acknowledged.

■ REFERENCES

(1) Huber, G. W.; Iborra, S.; Corma, A. *Chem. Rev.* **2006**, *106*, 4044−4098.
(2) Lynd, L. R. *Annu. Rev. Energy Env.* **1996**, *21*, 403−465.
(3) Iglesia, E.; Reyes, S. C.; Madon, R. J.; Soled, S. L. *Adv. Catal.* **1993**, *39*, 221−302.
(4) Khodakov, A. Y.; Chu, W.; Fongarland, P. *Chem. Rev.* **2007**, *107*, 1692−1744.
(5) Ponec, V. *Catal. Rev.: Sci. Eng.* **1978**, *18*, 151−171.
(6) Spivey, J. J.; Egbebi, A. *Chem. Soc. Rev.* **2007**, *36*, 1514−1528.
(7) Subramani, V.; Gangwal, S. K. *Energy Fuels* **2008**, *22*, 814−839.
(8) Van der Laan, G. P.; Beenackers, A. *Catal. Rev.: Sci. Eng.* **1999**, *41*, 255−318.
(9) van der Lee, G.; Ponec, V. *Catal. Rev.: Sci. Eng.* **1987**, *29*, 183−218.
(10) Oshikawa, K.; Nagai, M.; Omi, S. *J. Phys. Chem. B* **2001**, *105*, 9124−9131.
(11) Claridge, J. B.; York, A. P. E.; Brungs, A. J.; Marquez-Alvarez, C.; Sloan, J.; Tsang, S. C.; Green, M. L. H. *J. Catal.* **1998**, *180*, 85−100.
(12) Barthos, R.; Solymosi, F. *J. Catal.* **2007**, *249*, 289−299.
(13) Kojima, I.; Miyazaki, E.; Yasumori, I. *J. Chem. Soc., Chem. Commun.* **1980**, 573−574.
(14) Oyama, S. T. *Catal. Today* **1992**, *15*, 179−200.
(15) Park, K. Y.; Seo, W. K.; Lee, J. S. *Catal. Lett.* **1991**, *11*, 349−356.
(16) Vo, D. V. N.; Adesina, A. A. *Appl. Catal., A* **2011**, *399*, 221−232.
(17) Griboval-Constant, A.; Giraudon, J. M.; Leclercq, G.; Leclercq, L. *Appl. Catal., A* **2004**, *260*, 35−45.
(18) Patt, J.; Moon, D. J.; Phillips, C.; Thompson, L. *Catal. Lett.* **2000**, *65*, 193−195.
(19) Moon, D. J.; Ryu, J. W. *Catal. Lett.* **2004**, *92*, 17−24.
(20) Nagai, M.; Matsuda, K. *J. Catal.* **2006**, *238*, 489−496.
(21) Woo, H. C.; Park, K. Y.; Kim, Y. G.; Nam, I. S.; Chung, J. S.; Lee, J. S. *Appl. Catal.* **1991**, *75*, 267−280.
(22) Xiang, M. L.; Li, D. B.; Li, W. H.; Zhong, B.; Sun, Y. H. *Fuel* **2006**, *85*, 2662−2665.
(23) Shou, H.; Davis, R. J. *J. Catal.* **2011**, *282*, 83−93.
(24) Shou, H.; Li, L.; Ferrari, D.; Sholl, D. S.; Davis, R. J. *J. Catal.* **2013**, *299*, 150−161.
(25) Kitchin, J. R.; Norskov, J. K.; Barteau, M. A.; Chen, J. G. G. *Catal. Today* **2005**, *105*, 66−73.
(26) Han, J. W.; Li, L.; Sholl, D. S. *J. Phys. Chem. C* **2011**, *115*, 6870−6876.
(27) Pistonesi, C.; Juan, A.; Farkas, A. P.; Solymosi, F. *Surf. Sci.* **2008**, *602*, 2206−2211.
(28) Ren, J.; Huo, C. F.; Wang, J. G.; Li, Y. W.; Jiao, H. J. *Surf. Sci.* **2005**, *596*, 212−221.
(29) Shi, X. R.; Wang, S. G.; Wang, H.; Deng, C. M.; Qin, Z. F.; Wang, J. G. *Surf. Sci.* **2009**, *603*, 852−859.
(30) Hugosson, H. W.; Eriksson, O.; Nordstrom, L.; Jansson, U.; Fast, L.; Delin, A.; Wills, J. M.; Johansson, B. *J. Appl. Phys.* **1999**, *86*, 3758−3767.
(31) Wang, T.; Liu, X. W.; Wang, S. G.; Huo, C. F.; Li, Y. W.; Wang, J. G.; Jiao, H. J. *J. Phys. Chem. C* **2011**, *115*, 22360−22368.
(32) Shi, X.-R.; Wang, J.; Hermann, K. *J. Phys. Chem. C* **2010**, *114*, 13630−13641.
(33) Tominaga, H.; Nagai, M. *J. Phys. Chem. B* **2005**, *109*, 20415−20423.
(34) Tominaga, H.; Nagai, M. *Appl. Catal., A* **2005**, *282*, 5−13.
(35) Vojvodic, A. *Catal. Lett.* **2012**, *142*, 728−735.
(36) Medford, A. J.; Vojvodic, A.; Studt, F.; Abild-Pedersen, F.; Norskov, J. K. *J. Catal.* **2012**, *290*, 108−117.
(37) Pistonesi, C.; Pronsato, M. E.; Bugyi, L.; Juan, A. *J. Phys. Chem. C* **2012**, *116*, 24573−24581.
(38) Tominaga, H.; Aoki, Y.; Nagai, M. *Appl. Catal., A* **2012**, *423-424*, 192−204.
(39) Kresse, G.; Furthmuller, J. *Phys. Rev. B: Condens. Matter Mater. Phys.* **1996**, *54*, 11169−11186.
(40) Kresse, G.; Hafner, J. *Phys. Rev. B: Condens. Matter Mater. Phys.* **1993**, *47*, 558−561.

DOI: 10.1021/acscatal.5b00419
ACS Catal. 2015, 5, 5174−5185

(41) Kresse, G.; Hafner, J. *J. Phys.: Condens. Matter* **1994**, *6*, 8245−8257.
(42) Sholl, D. S.; Steckel, J. A. *Density functional theory: a practical introduction*; John Wiley & Sons, Inc.: Hoboken, NJ, 2009.
(43) Perdew, J. P.; Burke, K.; Ernzerhof, M. *Phys. Rev. Lett.* **1996**, *77*, 3865−3868.
(44) Perdew, J. P.; Burke, K.; Ernzerhof, M. *Phys. Rev. Lett.* **1997**, *78*, 1396−1396.
(45) Blöchl, P. E. *Phys. Rev. B: Condens. Matter Mater. Phys.* **1994**, *50*, 17953.
(46) Kresse, G.; Joubert, D. *Phys. Rev. B: Condens. Matter Mater. Phys.* **1999**, *59*, 1758−1775.
(47) Bengtsson, L. *Phys. Rev. B: Condens. Matter Mater. Phys.* **1999**, *59*, 12301−12304.
(48) Neugebauer, J.; Scheffler, M. *Phys. Rev. B: Condens. Matter Mater. Phys.* **1992**, *46*, 16067−16080.
(49) Lo, R. L.; Fukui, K.; Otani, S.; Iwasawa, Y. *Surf. Sci.* **1999**, *440*, L857−L862.
(50) Lo, R. L.; Fukui, K.; Otani, S.; Oyama, S. T.; Iwasawa, Y. *Jpn. J. Appl. Phys., Part 1* **1999**, *38*, 3813−3815.
(51) Newsome, D. S. *Catal. Rev.: Sci. Eng.* **1980**, *21*, 275−318.
(52) Ratnasamy, C.; Wagner, J. P. *Catal. Rev.: Sci. Eng.* **2009**, *51*, 325−440.
(53) Rhodes, C.; Hutchings, G. J.; Ward, A. M. *Catal. Today* **1995**, *23*, 43−58.
(54) Chinchen, G. C.; Denny, P. J.; Jennings, J. R.; Spencer, M. S.; Waugh, K. C. *Appl. Catal.* **1988**, *36*, 1−65.
(55) Klier, K. *Adv. Catal.* **1982**, *31*, 243−313.
(56) Liu, X. M.; Lu, G. Q.; Yan, Z. F.; Beltramini, J. *Ind. Eng. Chem. Res.* **2003**, *42*, 6518−6530.
(57) Forzatti, P.; Tronconi, E.; Pasquon, I. *Catal. Rev.: Sci. Eng.* **1991**, *33*, 109−168.
(58) Cheng, J.; Gong, X. Q.; Hu, P.; Lok, C. M.; Ellis, P.; French, S. *J. Catal.* **2008**, *254*, 285−295.
(59) Cheng, J.; Hu, P.; Ellis, P.; French, S.; Kelly, G.; Lok, C. M. *J. Phys. Chem. C* **2008**, *112*, 9464−9473.
(60) Cheng, J.; Hu, P.; Ellis, P.; French, S.; Kelly, G.; Lok, C. M. *J. Phys. Chem. C* **2008**, *112*, 6082−6086.
(61) Cheng, J.; Hu, P.; Ellis, P.; French, S.; Kelly, G.; Lok, C. M. *J. Catal.* **2008**, *257*, 221−228.
(62) Cheng, J.; Hu, P.; Ellis, P.; French, S.; Kelly, G.; Lok, C. M. *Top. Catal.* **2010**, *53*, 326−337.
(63) Choi, Y.; Liu, P. *J. Am. Chem. Soc.* **2009**, *131*, 13054−13061.
(64) Grabow, L. C.; Mavrikakis, M. *ACS Catal.* **2011**, *1*, 365−384.
(65) Gokhale, A. A.; Dumesic, J. A.; Mavrikakis, M. *J. Am. Chem. Soc.* **2008**, *130*, 1402−1414.
(66) Madon, R. J.; Braden, D.; Kandoi, S.; Nagel, P.; Mavrikakis, M.; Dumesic, J. A. *J. Catal.* **2011**, *281*, 1−11.
(67) Grabow, L. C.; Gokhale, A. A.; Evans, S. T.; Dumesic, J. A.; Mavrikakis, M. *J. Phys. Chem. C* **2008**, *112*, 4608−4617.
(68) Ferrin, P.; Simonetti, D.; Kandoi, S.; Kunkes, E.; Dumesic, J. A.; Norskov, J. K.; Mavrikakis, M. *J. Am. Chem. Soc.* **2009**, *131*, 5809−5815.
(69) Mei, D.; Rousseau, R.; Kathmann, S. M.; Glezakou, V.-A.; Engelhard, M. H.; Jiang, W.; Wang, C.; Gerber, M. A.; White, J. F.; Stevens, D. J. *J. Catal.* **2010**, *271*, 325−342.
(70) Fischer, F.; Tropsch, H. *Ber. Dtsch. Chem. Ges. B* **1926**, *59*, 830−831.
(71) Ponec, V. *Catal. Today* **1992**, *12*, 227−254.
(72) Orita, H.; Naito, S.; Tamaru, K. *J. Catal.* **1984**, *90*, 183−193.
(73) Chinchen, G. C.; Denny, P. J.; Parker, D. G.; Spencer, M. S.; Whan, D. A. *Appl. Catal.* **1987**, *30*, 333−338.
(74) Waugh, K. C. *Catal. Today* **1992**, *15*, 51−75.
(75) Rasmussen, P. B.; Kazuta, M.; Chorkendorff, I. *Surf. Sci.* **1994**, *318*, 267−380.
(76) Rasmussen, P. B.; Holmblad, P. M.; Askgaard, T.; Ovesen, C. V.; Stoltze, P.; Norskov, J. K.; Chorkendorff, I. *Catal. Lett.* **1994**, *26*, 373−381.
(77) Koryabkina, N. A.; Phatak, A. A.; Ruettinger, W. F.; Farrauto, R. J.; Ribeiro, F. H. *J. Catal.* **2003**, *217*, 233−239.
(78) Ovesen, C. V.; Clausen, B. S.; Hammershoi, B. S.; Steffensen, G.; Askgaard, T.; Chorkendorff, I.; Norskov, J. K.; Rasmussen, P. B.; Stoltze, P.; Taylor, P. *J. Catal.* **1996**, *158*, 170−180.
(79) Ovesen, C. V.; Stoltze, P.; Norskov, J. K.; Campbell, C. T. *J. Catal.* **1992**, *134*, 445−468.
(80) Shou, H.; Ferrari, D.; Barton, D. G.; Jones, C. W.; Davis, R. J. *ACS Catal.* **2012**, *2*, 1408−1416.
(81) Hammer, B.; Hansen, L. B.; Norskov, J. K. *Phys. Rev. B: Condens. Matter Mater. Phys.* **1999**, *59*, 7413−7421.
(82) Bugyi, L.; Solymosi, F. *J. Phys. Chem. B* **2001**, *105*, 4337−4342.
(83) Redhead, P. A. *Vacuum* **1962**, *12*, 203−211.
(84) Michaelides, A.; Liu, Z. P.; Zhang, C. J.; Alavi, A.; King, D. A.; Hu, P. *J. Am. Chem. Soc.* **2003**, *125*, 3704−3705.
(85) Sutton, J. E.; Vlachos, D. G. *ACS Catal.* **2012**, *2*, 1624−1634.
(86) van Santen, R. A.; Neurock, M.; Shetty, S. G. *Chem. Rev.* **2010**, *110*, 2005−2048.
(87) Wang, S. G.; Temel, B.; Shen, J. A.; Jones, G.; Grabow, L. C.; Studt, F.; Bligaard, T.; Abild-Pedersen, F.; Christensen, C. H.; Norskov, J. K. *Catal. Lett.* **2011**, *141*, 370−373.
(88) Reuter, K.; Scheffler, M. *Phys. Rev. B: Condens. Matter Mater. Phys.* **2006**, *73*, 045433.
(89) Datar, A. S.; Prasad, S. D. *Langmuir* **1991**, *7*, 1310−1313.
(90) King, D. A.; Wells, M. G. *Proc. R. Soc. London, Ser. A* **1974**, *339*, 245−269.
(91) Fowler, R. H.; Guggenheim, E. A. *Statistical Thermodynamics*; Cambridge University Press: London, 1965.
(92) Vannice, M. A. *Kinetics of Catalytic Reactions*, 1st ed.; Springer: New York, 2005.
(93) Bouchy, C.; Pham-Huu, C.; Heinrich, B.; Chaumont, C.; Ledoux, M. J. *J. Catal.* **2000**, *190*, 92−103.
(94) Delporte, P.; Meunier, F.; Phamhuu, C.; Vennegues, P.; Ledoux, M. J.; Guille, J. *Catal. Today* **1995**, *23*, 251−267.
(95) Edamoto, K.; Sugihara, M.; Ozawa, K.; Otani, S. *Surf. Sci.* **2004**, *561*, 101−109.
(96) Liu, P.; Rodriguez, J. A. *J. Phys. Chem. B* **2006**, *110*, 19418−19425.
(97) Oyama, S. T.; Delporte, P.; PhamHuu, C.; Ledoux, M. J. *Chem. Lett.* **1997**, 949−950.
(98) Wu, W. C.; Wu, Z. L.; Liang, C. H.; Chen, X. W.; Ying, P. L.; Li, C. *J. Phys. Chem. B* **2003**, *107*, 7088−7094.
(99) Zaman, S.; Smith, K. J. *Catal. Rev.: Sci. Eng.* **2012**, *54*, 41−132.
(100) Bell, A. T. *Catal. Rev.: Sci. Eng.* **1981**, *23*, 203−232.
(101) Ojeda, M.; Nabar, R.; Nilekar, A. U.; Ishikawa, A.; Mavrikakis, M.; Iglesia, E. *J. Catal.* **2010**, *272*, 287−297.
(102) Huo, C.-F.; Ren, J.; Li, Y.-W.; Wang, J.; Jiao, H. *J. Catal.* **2007**, *249*, 174−184.
(103) Andersson, M. P.; Abild-Pedersen, E.; Remediakis, I. N.; Bligaard, T.; Jones, G.; Engbaek, J.; Lytken, O.; Horch, S.; Nielsen, J. H.; Sehested, J.; Rostrup-Nielsen, J. R.; Norskov, J. K.; Chorkendorff, I. *J. Catal.* **2008**, *255*, 6−19.
(104) Campbell, C. T. *Top. Catal.* **1994**, *1*, 353−366.
(105) Campbell, C. T. *J. Catal.* **2001**, *204*, 520−524.

DOI: 10.1021/acscatal.5b00419
ACS Catal. 2015, 5, 5174−5185